ChemCatChem | doi.org/10.1002/cctc.202000329

Visible Light-driven Dehydrogenation of Benzylamine under Liberation of H_2

Mara Klarner,[a] Sebastian Hammon,[b] Sebastian Feulner,[c] Stephan Kümmel,[b] Lothar Kador,[c] and Rhett Kempe*[a]

The visible light-driven transformation of chemical compounds in combination with the liberation of H_2 is highly attractive. Herein, we report on a photocatalyst that allows the acceptorless dehydrogenation of benzylamine. Upon light absorption, free charge carriers are generated and used for the concerted imine formation and liberation of H_2. Our photocatalyst consists of CdS as a light harvesting semiconductor supported on colloidal metal-organic framework crystallites. The decoration with co-catalytic nickel nanoparticles promotes hydrogen evolution and, in addition, stabilizes the CdS component under irradiation.

Introduction

The solar-driven upgrading of organic compounds is a promising and sustainable way to produce value-added products.[1] The simultaneous liberation of H_2 during such upgrading processes generates an additional, highly attractive byproduct. Meanwhile, a well investigated approach is the photocatalytic acceptorless dehydrogenation of alcohols (alcohol splitting) to yield carbonyl compounds (Scheme 1, top).[2] In a similar way, amines may be transformed into imines and H_2 (Scheme 1, bottom). The photocatalytic amine dehydrogenation described so far requires sacrificial agents, mostly molecular oxygen (aerobic amine oxidation). The visible light-mediated aerobic amine oxidation is catalyzed by semiconductor materials including CdS,[3] graphitic carbon nitride,[4] Nb_2O_5,[5] WS_2,[6] WO_3[7] and bismuth oxyhalides.[8] Zhao and coworkers developed a Ni/CdS catalyst system for the visible light-driven H_2 generation from water in combination with the coupling of amines.[9] Furthermore, heterojunction photocatalysts,[10] plasmonic composite catalysts[11] and MOF-based photocatalysts[12] are described to yield homocoupled imines via aerobic amine oxidation. The transformation of two different amines into a non-symmetric imine is more challenging, requiring high temperatures and oxygen pressure.[13]

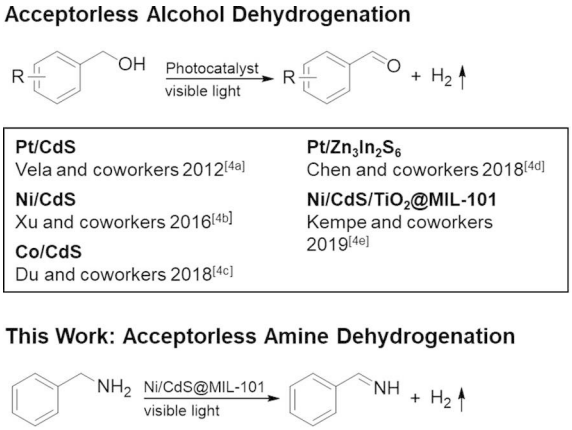

Scheme 1. State of the art in visible light-mediated photocatalytic dehydrogenation of alcohols with liberation of H_2 (alcohol splitting) and the acceptorless dehydrogenation of benzylamine (amine splitting) introduced here.

Herein, we report on the photocatalytic and visible light-driven acceptorless dehydrogenation of benzylamine (amine splitting). The reaction proceeds additive-free, without requiring an electron acceptor, and involves amine oxidation towards an imine in combination with liberation of one equivalent of H_2. The synthesis of non-symmetric imines is possible by using a second, non-benzylic amine that is not dehydrogenated by the photocatalyst. To accomplish amine splitting, we developed a novel metal-organic framework-based photocatalyst system (Ni/CdS@MIL-101).

Ni/CdS@MIL-101 is composed of three components. a) The metal organic framework (MOF) known as MIL-101(Cr) is used as the visible light inactive support material that acts as a molecular sponge permitting the semiconductor and catalyst synthesis and determines the overall size of the photocatalyst for efficient recycling.[14] b) CdS is the visible light absorbing semiconductor material. c) Nickel nanoparticles are an efficient

[a] M. Klarner, Prof. Dr. R. Kempe
Inorganic Chemistry II
University of Bayreuth
Universitätsstraße 30, 95440 Bayreuth (Germany)
E-mail: kempe@uni-bayreuth.de
[b] S. Hammon, Prof. Dr. S. Kümmel
Theoretical Physics IV
University of Bayreuth
Universitätsstraße 30, 95447 Bayreuth (Germany)
[c] S. Feulner, Prof. Dr. L. Kador
Institute of Physics, Bayreuth Institute of Macromolecule Research (BIMF)
University of Bayreuth
Universitätsstraße 30, 95447 Bayreuth (Germany)

Supporting information for this article is available on the WWW under https://doi.org/10.1002/cctc.202000329

co-catalyst for H_2 evolution and enhance the stability of CdS under photocatalytic conditions since the oxidation of sulfide to sulfate is prevented. Fluorescence lifetime measurements indicate a faster electron transfer from the conduction band of CdS to the Ni particles in comparison to nanoparticles of noble metals such as Pd or Pt. Thereby, the probability of charge recombination within the semiconductor is reduced. In addition, DFT calculations suggest a stronger substrate binding of the amine to the Ni than to Pd nanoparticles.

Results and Discussion

The photocatalytically inactive MOF MIL-101 with its characteristic pore structure (Supporting Information, Figure S2a) was shown to have a surface area of 2700 m^2/g.[15] The MIL-101 crystallite size, between 100 and 300 nm, is desirable for the generation of active and reusable core-shell catalysts. The MIL-101 crystallites are small enough to exhibit a proper outer surface area for the modification with photoactive components.[16] This is combined with the easy separation of the colloidal photocatalyst, since the crystallites are, on the other hand, large enough to ensure recyclability by centrifugation. The highly porous and size optimized support material can be selectively loaded with precursor molecules permitting the catalyst synthesis. The outer surface of single MIL-101 crystallites is decorated with visible light-absorbing CdS particles by a simple solvothermal route. Cadmium acetate is infiltrated into MIL-101 in dimethyl sulfoxide as sulfur source and crystallizes as cubic CdS under solvothermal conditions at 180 °C to yield CdS@MIL-101.[17] Transmission electron microscopy revealed the arrangement of CdS particles with an average size between 20 and 30 nm on the structure determining core MIL-101 (Scheme 2; Supporting Information, Figure S4). The gas phase infiltration of volatile metal-organic precursors into the porous CdS@MIL-101 composite material allows for the generation of metal nanoparticles, denoted as M/CdS@MIL-101. For the modification with nickel nanoparticles, bis(cyclopentadienyl) nickel(II) [$Ni(C_5H_5)_2$] was infiltrated at room temperature by applying static vacuum and subsequently reducing to Ni_0 at 90 °C and 10 bar H_2.[18] We modified CdS@MIL-101 with different amounts of nickel, 1 wt.%, 5 wt.%, and 10 wt.%. (η_3-Allyl)(η_5-cyclopentadienyl)-palladium(II) [$Pd(C_3H_5)(C_5H_5)$] was used to generate 5 wt.% Pd_0 nanoparticles by sublimation at 32 °C in dynamic vacuum and reduction at 70 °C and 70 bar H_2.[19] The modification with 5 wt.% Pt_0 proceeds via the gas phase loading of trimethyl-(methylcyclopentadienyl)-palladium(IV) [$Me_3Pt(CH_3$-$C_5H_4)$] into the pores of CdS@MIL-101 at 37 °C in static vacuum, followed by a reduction step at 80 °C and 50 bar H_2.[20] TEM analysis (Scheme 2; Supporting Information, Figure S3) indicated a homogeneous distribution of metallic nanoparticles smaller than 2 nm which are located on the CdS particles, forming an interface with the visible light-absorbing semiconducting material. The metal content of M_5CdS@MIL-101 catalysts (theoretically 5 wt.%) was examined by inductively coupled plasma optical emission spectroscopy (ICP-OES) and found to be 5.1 wt.% Ni, 5.2 wt.% Pd, and 4.9 wt.% Pt, respectively (Supporting Information, Table S1). The calculated weight percentage of CdS is 45 wt.% for each catalyst material. The final M/CdS@MIL-101 core-shell composite showed the original octahedral shape determined by the MIL-101. The metal nanoparticles are assumed to serve as an electron reservoir, since a directed electron transfer from the conduction band of the semiconductor CdS across the semiconductor/nanoparticle interface has been postulated.[21] Scheme 2 presents the general photocatalytic concept of M/CdS@MIL-101: An electron-hole pair is generated upon visible light excitation of CdS. The electron is transferred from the conduction band (CB) of CdS to a metal particle by the built-in electric field, thereby reducing the possibility of charge recombination. Subsequently, spatially separated redox reactions can be catalyzed. Electrons reduce protons for molecular hydrogen generation at the co-catalytic nanoparticles and, simultaneously, holes in the CdS valence band are consumed by oxidizing substrates.

For determining the absorbance characteristics of Ni_5CdS@MIL-101, we performed diffuse-reflectance ultraviolet-

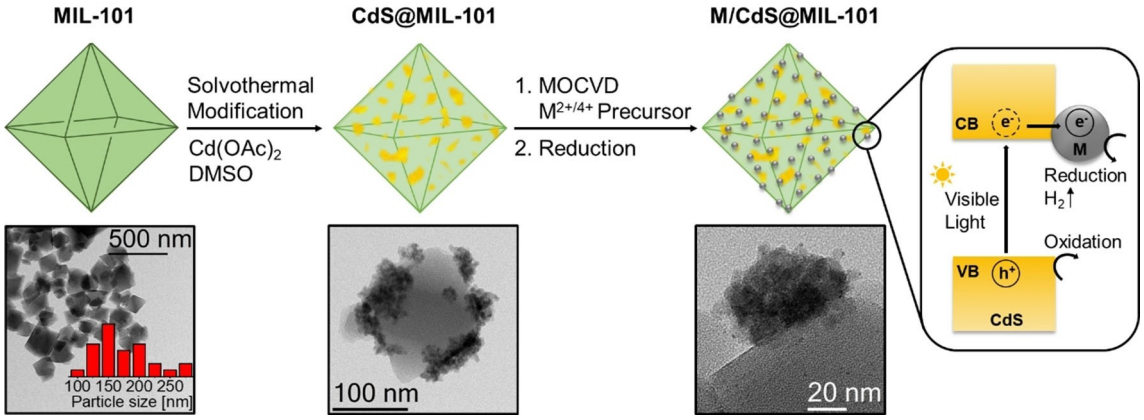

Scheme 2. Synthesis of the photocatalyst M/CdS@MIL-101. The decoration with CdS semiconductor particles proceeds via a solvothermal modification. The metal precursor (Ni: [$Ni(C_5H_5)_2$]; Pd: [$Pd(C_3H_5)(C_5H_5)$]; Pt: [$Me_3Pt(CH_3$–$C_5H_4)$]) is infiltrated into MIL-101 (green) by gas phase deposition and reduced by hydrogen treatment. In the semiconductor CdS (yellow) an electron is promoted from the valence band (VB) to the conduction band (CB) by the absorption of visible light. After the directed electron transfer towards the metal particles (grey), spatially separated redox reactions can be catalyzed.

visible spectroscopy (DRS) between 350 and 700 nm. As compared to bare MIL-101 absorbing around 600 and 450 nm, an increased absorption was observed for the dark yellow CdS@MIL-101 (Supporting Information, Figure S4a). Upon generating the photoactive compound, the characteristic absorbance of MIL-101 is extinguished. Photons of wavelengths smaller than 510 nm are predominantly absorbed, corresponding to the band gap of the semiconductor CdS. With the Munk-Kubelka equation, the optical band gap of CdS was determined as 2.44 eV, in agreement with the literature value for cubic CdS (Supporting Information, Figure S4b). The photocatalyst Ni_5CdS@MIL-101 exhibited nearly constant absorbance throughout the visible range. We examined the surface area and the pore size distribution of the different compounds during synthesis of the photocatalyst by nitrogen physisorption measurements. The modification of porous MIL-101 with CdS results in a significant decrease of the initial surface area by 53%. Further modification with Ni nanoparticles leads only to a minor additional decrease of the surface area to 1040 m^2/g. X-ray powder diffractometry (PXRD) reveals the exclusive formation of cubic CdS particles (Supporting Information, Figure S8a) showing reflections at 26.5°, 43.9°, and 51.9° (2θ). The reflections from 2° to 20° (2θ) are assigned to the preserved MIL-101 core. X-ray photoelectron spectroscopy (XPS) indicated the formation of metallic Ni nanoparticles (Supporting Information, Figure S5). The major peak within the S2p region at a binding energy of 161.5 eV is assigned to metallic sulfide (CdS). Traces of metal sulfate were identified at a binding energy of 169 eV; they are ascribed to surface oxidation of CdS due to the handling in air. The XPS survey shows characteristic elemental signals for Cr, O, and C of the MIL-101 support material and additional signals for Cd, S, and Ni, which form the photoactive shell. The homogeneous distribution of Ni particles on the CdS@MIL-101 material was confirmed by energy dispersive X-ray (EDX) elemental mapping (Supporting Information, Figure S6). Furthermore, we performed Fourier-transform infrared spectroscopy (FT-IR) of Ni_5CdS@MIL-101 and the intermediate materials during synthesis (Supporting Information, Figure S7a). Due to the surface modification with the light harvesting CdS, MIL-101 signals are reduced between 700 and 2000 cm^{-1}. A total weight loss of 42% was observed for the Ni_5CdS@MIL-101 photocatalyst as compared to 72% for MIL-101 in thermogravimetric analysis (TGA) (Supporting Information, Figure S7b). By covering the MOF core with the photocatalytic active shell, the temperature stability of the system is enhanced.

Next, we performed the photocatalytic acceptorless dehydrogenation of benzylamine via liberation of molecular H_2. Thereby, the intermediate aldimine reacts with a second equivalent of benzylamine in a condensation reaction to yield the homocoupled product *N*-benzyl-1-phenylmethanimine (Figure 1a). The elimination of gaseous ammonia was verified by gas chromatography (thermal conductive detector, GC-TCD). The flat band potential of CdS is sufficiently positive (VB 1.7 V vs NHE)[22] to thermodynamically allow for the oxidation of benzylamine (standard reduction potential 0.9 V vs NHE).[23] The photocatalytic amine dehydrogenation by Ni_5CdS@MIL-101 was performed under an inert-gas atmosphere at room temperature

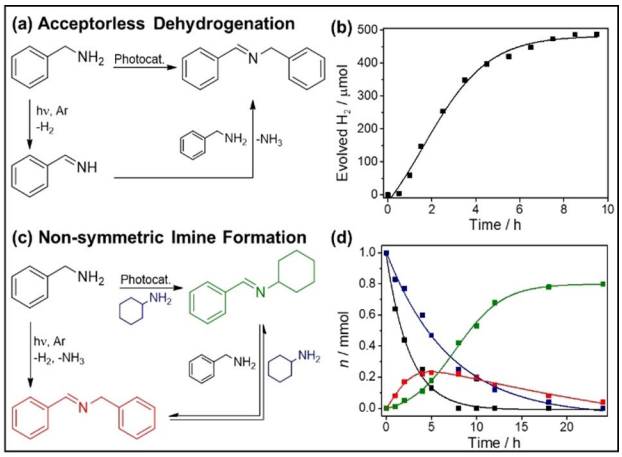

Figure 1. (a) Acceptorless dehydrogenation of benzylamine. (b) H_2 liberation from benzylamine (1 mmol) is observed under visible light illumination and quantified by GC-TCD. (c) Non-symmetric imine formation by cross-coupling benzylamine and cyclohexylamine. (d) Kinetic study (color code refers to (c)).

without the use of any additives or acceptor molecules. In the presence of co-catalytic Ni nanoparticles, the dehydrogenation of benzylamine proceeds with quantitative yield, whereas the neat CdS@MIL-101 leads to the formation of the tertiary amine as a byproduct (Table 1, Entry 1, 2). We confirmed the equimolar liberation of molecular H_2 by analyzing the reaction headspace via GC-TCD (Figure 1b). Switching the light on and off verified the release of H_2 only under visible light illumination (Supporting Information, Figure S10). The reusability of Ni_5CdS@MIL-101 photocatalyst was investigated by the acceptorless dehydrogenation of benzylamine. We performed five consecutive runs without a remarkable loss of activity (Supporting Information, Figure S11).

We also developed an approach to access non-symmetric imines using a second, non-benzylic amine which is not dehydrogenated by the photocatalyst under the given conditions. Figure 1c describes the cross-coupling of benzylamine and cyclohexylamine via the dehydrogenation of benzylamine and subsequent reversible transimination to yield the hetero-coupled *N*-cyclohexyl-1-phenylmethanimine (Figure 1c, d). This exchange is a non-photocatalytic equilibrium reaction, in which one equivalent of benzylamine is liberated and fed back into

Table 1. Photocatalytic acceptorless dehydrogenation of benzylamine.[a]

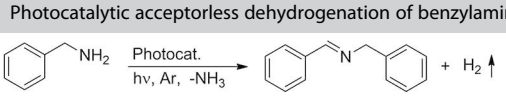

	Catalyst	Yield [%][b]	Yield H_2 [%][c]
1	Ni_5CdS@MIL-101	99	98
2	CdS@MIL-101	62	59
3	Without *hν*	0	0
4	Without catalyst	0	0

[a] 1 mmol benzylamine, 1.5 mL MeCN, 10 h, 5 mg catalyst, rt, Ar, 470 nm blue LED (50 W). [b] Determined by GC using n-dodecane as an internal standard. [c] Quantified by GC-TDC using methane as an internal standard.

the dehydrogenation cycle. Under visible light illumination, the equilibrium is shifted towards the non-symmetric imine, guaranteeing its predominant formation (Supporting Information, Table S5).

We synthesized the Ni_xCdS@MIL-101 catalyst systems with different Ni contents (x equal to 1, 5, 10 wt.% Ni) to investigate the influence of the co-catalytic nanoparticles on the dehydrogenative cross-coupling. To convert 1 mmol of substrates under optimized reaction conditions, 5 mg Ni_5CdS@MIL-101 were suspended in 1.5 ml ethanol and illuminated with a 50 W blue LED (470 nm) (Supporting Information, Figure S1, Table S3 and S4).

CdS@MIL-101 loaded with 5 wt.% Ni showed the best catalytic performance yielding 74% heterocoupled product **1** and 7% homocoupled product **2** (Table 2, Entry 2). With increasing Ni content, the nanoparticles covering the CdS crystals reduce the light absorbance and, thereby, the generation of free charge carriers resulting in 17% of **1** and 37% of **2** (Table 2, Entry 3). With 1 wt.% Ni, the photocatalytic activity is similar to neat CdS@MIL-101 (Table 2, Entry 1). The MIL-101 support is essential, since Ni-modified commercial CdS shows a significantly lower activity (Table 2, Entry 4). Also, the unmodified CdS@MIL-101 shows a lower catalytic activity (Table 2, Entry 5) underlining the importance of Ni nanoparticles which was already observed for the formation of the homocoupled product *N*-benzyl-1-phenylmethanimine **2**. We found no photocatalytic activity without the light-harvesting CdS component in both Ni@MIL-101 and the neat support MIL-101 (Table 2, Entries 6, 7). The modification with the noble metals Pd and Pt as co-catalysts leads mainly to the formation of the homocoupled product **2** (Table 2, Entries 8, 9). This fact highlights the superior performance of co-catalytic non-noble Ni nanoparticles. The composite material Ni_5CdS@MIL-101 catalyzes the cross-coupling of amines as shown by several control experiments: Without the catalyst and without visible light illumination no conversion of the substrates occurs(Table 2, Entries 10, 11). Interestingly, a significantly reduced yield is observed in air (Table 2, Entry 12).

Next, we studied the stability of the semiconducting CdS component of Ni_5CdS@MIL-101 under photocatalytic conditions. The corrosion of CdS is a frequently discussed phenomenon and a main challenge in the use of such photocatalysts.[24] Recently, DiMeglio and co-workers reported on the benzylamine mediated oxidation of sulfide during the non-aqueous dehydrogenation of benzylamine with O_2 as a sacrificial agent.[25] The standard reduction potential of benzylamine thermodynamically allows for the oxidation of CdS via the formation of the amine-radical cation. In a typical photocatalytic set-up, the photocatalysts Ni_5CdS@MIL-101 and CdS@MIL-101 were illuminated in the presence of benzylamine and ethanol as solvent in an inert gas atmosphere.

The pre-catalytic CdS@MIL-101 exhibits one major sulfur signal at $^2P_{3/2}$ 161.5 eV (86%) corresponding to metal sulfide and a small signal for metal sulfate at $^2P_{3/2}$ 168.7 eV (14%) (Figure 2, (1) and (2)). Post-catalytic PXRD analysis indicates the formation of oxidized sulfur species due to the presence of several reflections besides those of cubic CdS (Supporting Information, Figure S8). XPS analysis in the S^2p region confirms an increase in surface sulfate to 51%. The modification with Ni nanoparticles improves the stability of the CdS component since no corrosion effects are observed in PXRD. The ratio of CdS (94%) to $CdSO_4$ (6%) is constant for pre- and post-catalytic Ni_5CdS@MIL-101 (Figure 2, (3) and (4)). We performed several control experiments without either visible light illumination, or the presence of benzylamine or solvent and, in addition, in dry

Table 2. Photocatalytic dehydrogenation of benzylamine and cross-coupling with cyclohexylamine. Comparison of different Ni contents, different metal nanoparticles and different reaction conditions.[a]

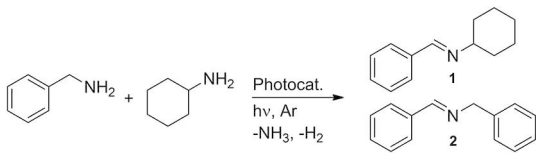

	Catalyst	Metal [wt %][b]	Yield 1 [%][c]	Yield 2 [%][c,d]
1	Ni_1CdS@MIL-101	1	45	12
2	Ni_5CdS@MIL-101	5.1[e]	74	7
3	Ni_{10}CdS@MIL-101	10	17	37
4	Ni@CdS[f]	5	18	4
5	CdS@MIL-101	–	42	17
6	Ni@MIL-101	5	0	0
7	MIL-101	–	0	0
8	Pd_5CdS@MIL-101	5.2[e]	8	34
9	Pt_5CdS@MIL-101	4.9[e]	7	51
10	Without hν	5.1[e]	0	0
11	Without catalyst	–	0	0
12	Ambient air	5.1[e]	11	23

[a] 1 mmol benzylamine, 1 mmol cyclohexylamine, 1.5 mL EtOH, 5 mg catalyst, 470 nm blue LED (50 W), 20 h, rt, Ar. [b] Co-catalytic metal nanoparticles (Ni, Pd, Pt). [c] Determined by GC using n-dodecane as an internal standard. [d] Referred to 0.5 mmol. [e] Determined by ICP-OES analysis. [f] Commercial CdS (Alfa Aesar).

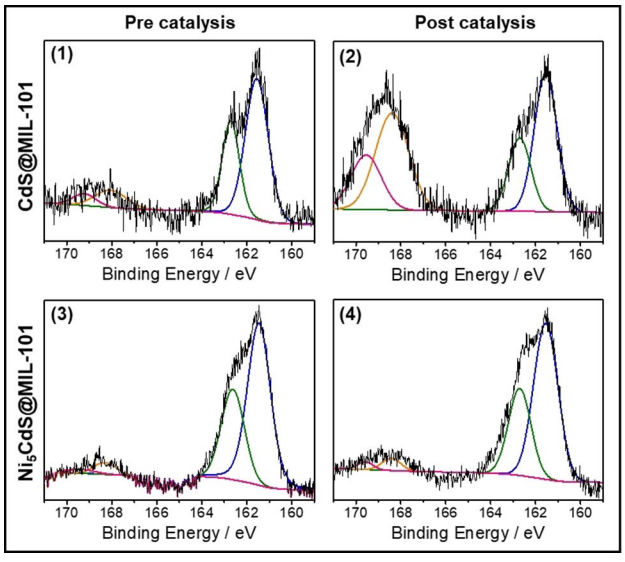

Figure 2. XPS studies of Ni_5CdS@MIL-101 and CdS@MIL-101 demonstrating the enhanced photocatalytic stability of CdS in the presence of Ni nanoparticles. Ni_5CdS@MIL-101 does not show significant degradation of the surface of CdS [(3), (4)], whereas CdS in CdS@MIL-101 is oxidized under photocatalytic conditions [(1), (2)]. For details see text.

acetonitrile. PXRD analysis of post-catalytic Ni_5CdS@MIL-101 materials showed no evidence for CdS corrosion in all these cases, which supports the idea of benzylamine-mediated sulfide oxidation in an oxygen-containing solvent (Supporting Information, Figure S8). The observed stability of CdS is decisive for the catalytic recyclability of Ni_5CdS@MIL-101. Further experiments on Pd_5CdS@MIL-101 and Pt_5CdS@MIL-101 photocatalysts revealed that the supposed stabilizing effect of metal nanoparticles on the CdS semiconductor occurs also with these noble metals.

The directed electron transfer from photo-excited CdS across the semiconductor-metal interface to Ni nanoparticles was investigated with fluorescence lifetime imaging microscopy in the frequency domain (FD-FLIM). A custom-built apparatus was used with a semiconductor laser at 487 nm and modulation frequencies between 110 and 155 MHz (adapted from Ref. [26]). The combination of the semiconductor material CdS with metallic particles opens up an additional decay channel of charge carriers in the conduction band of CdS. By absorbing visible light, an electron-hole pair is generated in the CdS component which can recombine after an intrinsic lifetime by emitting a photon. FD-FLIM data are conveniently plotted in the so-called polar-plot representation, where the quadrature component of the normalized fluorescence signal is plotted versus the component which is in phase with the excitation. Single-exponential decays correspond to data on a characteristic semi-circle with radius 0.5 around the point (0.5; 0) in this plot. Data points within the semi-circle, on the other hand, represent fluorescence decays featuring more than one lifetime component and can be linearly decomposed in the complex plane.[27] The photoluminescence lifetime of neat CdS supported on MIL-101 is determined by drawing a straight line through the data points in the polar plot and extrapolating it to the intersections with the semicircle (Figure 3a). Two lifetime components are extracted which are independent of the modulation frequency (Supporting Information, Figure S9). The shorter lifetime is interpreted as the luminescence lifetime of CdS, whereas the longer one is ascribed to the luminescence of the MIL-101. The position of the data points on the straight line represents the relative contributions of the two lifetime components to the luminescence signal. With increasing Ni content, the CdS lifetime gradually shortens from 115 ps (CdS@MIL-101) to 97 ps (Ni_1CdS@MIL-101), 67 ps (Ni_5CdS@MIL-101) and 11 ps ($Ni_{10}CdS$@MIL-101), respectively, verifying the directed electron transfer (Figure 3a-d). The relative variation of these lifetimes is reliable; the absolute numbers are subject to an uncertainty of about a factor two to three, however, given the comparatively low modulation frequencies. In accordance with the observed photocatalytic activity, the efficiency of the charge transfer increases with the Ni content. The charge carrier separation over two different catalyst components leads to the enhanced photocatalytic activity of Ni/CdS@MIL-101 in redox reactions. Comparing the 3d metal Ni with the noble metals Pd and Pt, the lifetime of neat CdS is most strongly affected by neighboring Ni particles, indicating faster electron transfer to Ni particles than to either Pd or Pt (Figure 3c, e, f). Comparing catalyst systems with 5 wt.% of the three metals, the lifetime of neat CdS is reduced from 115 ps to 108 ps (Pd_5CdS@MIL-101), 92 ps (Pt_5CdS@MIL-101) and 67 ps (Ni_5CdS@MIL-101). This result underlines the superior performance of Ni particles in the discussed photocatalytic reactions.

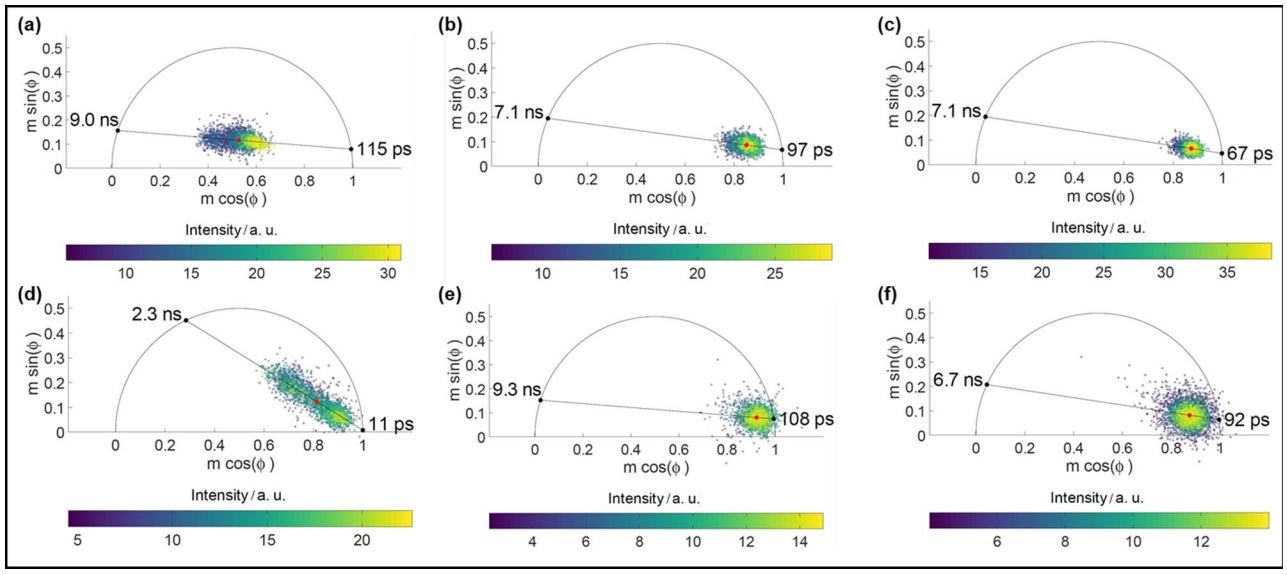

Figure 3. Fluorescence lifetime studies of MIL-101 supported catalysts confirming the directed electron transfer from excited CdS to Ni nanoparticles. Polar-plot representations of the data for Ni_xCdS@MIL-101 and M_5CdS@MIL-101: (a) neat CdS, (b) 1 wt.% Ni, (c) 5 wt.% Ni, (d) 10 wt.% Ni, (e) 5 wt.% Pd and (f) 5 wt.% Pt. The fluorescence lifetime of CdS decreases with increasing Ni content (right end point of the straight line on the semi-circle). It also depends on the metal nanoparticle (Ni, Pd, Pt; 5 wt.%) indicating an influence of the latter on the electron transfer efficiency. Data points correspond to diffraction-limited spots on the sample within an area of size 10×10 μm, the red dot indicating their center of mass. The fluorescence intensity of each spot is color-coded. The modulation frequency of the laser was 110 MHz. For further details see text.

In addition to a faster electron transfer from CdS to Ni in comparison to Pd or Pt particles, another reason for the superior photocatalytic performance of Ni/CdS@MIL-101 may be the interaction or binding of benzylamine with the metal nanoparticles. As a straightforward test we computed the binding energy of benzylamine to the metal nanoparticles. While this type of calculation can be performed using density functional theory (DFT) in principle, it requires careful considerations in practice: The structure of metal particles in general is difficult to determine due to the existence of many isomers of similar energy,[28] yet it may influence binding energies. Furthermore, common exchange-correlation approximations may reach their accuracy limits for d-electron systems.[29] For these reasons, we focused on 13-atom clusters of Ni and Pd as two representative test cases. Both form similar and stable cluster geometries, such as the icosahedron.[28,30] Our calculations suggest that the icosahedral structure is arguably the most relevant one for Ni_{13} and Pd_{13} at room temperature in solution (Supporting Information, Theoretical Procedure). Therefore, we investigated the binding energy of one benzylamine molecule to one 13-atom metal cluster (Ni_{13} or Pd_{13}) by computing the electronic and geometric structure using TURBOMOLE[31] (Supporting Information, Theoretical Procedure). We checked for possible limitations of the predictive power of the DFT calculations due to the presence of d-electrons by computing the binding energies with different exchange-correlation functionals.[32] In particular, the importance of localization and self-interaction was investigated by using functionals with different amounts of exact exchange.

We found the general trend that benzylamine binds stronger to Ni_{13} than to Pd_{13} by several hundred meV (Supporting Information, Table S8). The lowest energy geometries are depicted in Figure 4. This result correlates with a previous study on the binding energy of benzyl alcohol to Ni_{13} and Pd_{13}.[17a] Furthermore, we calculated the binding energy for the dehydrogenated intermediate (C_7H_7N). This intermediate also shows a higher binding energy to Ni_{13} than to Pd_{13}, yet overall slightly lower than benzylamine (Supporting Information, Theoretical Procedure).

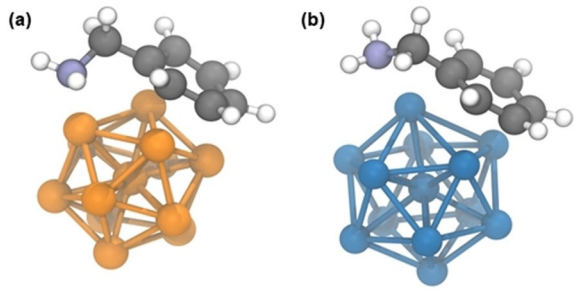

Figure 4. Lowest energy geometries obtained from Born-Oppenheimer DFT molecular dynamics simulations in which a benzylamine molecule binds to a 13-atom Pd icosahedral particle (a) and a 13-atom Ni icosahedral particle (b).

Conclusion

In conclusion, we have reported the first example of photocatalytic, visible light-driven acceptorless amine dehydrogenation (amine splitting). The noble metal-free photocatalyst Ni/CdS@MIL-101 oxidizes benzylamine with the liberation of one equivalent of H_2 most efficiently. The synthesis of non-symmetric imines is possible by adding a second amine which is not dehydrogenated by the photocatalyst under the given conditions. The MOF-supported colloidal photocatalyst is composed of the visible light-absorbing semiconductor CdS and Ni nanoparticles. We confirmed the directed electron transfer from the conduction band of CdS to metallic nanoparticles (Ni, Pd and Pt) and observed a faster electron transfer to the abundant non-noble metal Ni. The co-catalytic Ni (as well as Pd and Pt) also enhances the stability of CdS against photocorrosion in the presence of benzylamine. In addition, DFT calculations reveal a stronger binding of benzylamine to Ni than to Pd clusters.

Acknowledgements

This work was supported by the German Research Foundation (DFG SFB 840, B1). The authors also acknowledge the support of the Bavarian Polymer Institute (University of Bayreuth, KeyLab Electron and Optical Microscopy, KeyLab Theory and Simulation) and the initiative Solar Technologies go Hybrid. We thank Florian Puchtler (XRD) and Prof. Dr. Sven Hüttner (XPS). Furthermore, we thank the Elite Network Bavaria and the DAAD (Bayreuth-Melbourne Colloid/Polymer Network) for financial and other support. Open access funding enabled and organized by Projekt DEAL.

Conflict of Interest

The authors declare no conflict of interest.

Keywords: hydrogen generation · MOF · nickel · amines · photocatalysis

[1] G. Han, Y.-H. Jin, R. A. Burgess, N. E. Dickenson, X.-M. Cao, Y. Sun, *J. Am. Chem. Soc.* **2017**, *139*, 15584–15587.
[2] a) T. P. A. Ruberu, N. C. Nelson, I. I. Slowing, J. Vela, *J. Phys. Chem. Lett.* **2012**, *3*, 2798–2802; b) Z. Chai, T.-T. Zeng, Q. Li, L.-Q. Lu, W.-J. Xiao, D. Xu, *J. Am. Chem. Soc.* **2016**, *138*, 10128–10131; c) D. Jiang, X. Chen, Z. Zhang, L. Zhang, Y. Wang, Z. Sun, R. M. Irfan, P. Du, *J. Catal.* **2018**, *357*, 147–153; d) S. Meng, X. Ye, J. Zhang, X. Fu, S. Chen, *J. Catal.* **2018**, *367*, 159–170; e) D. Tilgner, M. Klarner, S. Hammon, M. Friedrich, A. Verch, N. de Jonge, S. Kümmel, R. Kempe, *Aust. J. Chem.* **2019**, *72*, 842–847; f) T. Mitkina, C. Stanglmair, W. Setzer, M. Gruber, H. Kisch, B. Koenig, *Org. Biomol. Chem.* **2012**, *10*, 3556–3561; g) K. Imamura, H. Tsukahara, K. Hamamichi, N. Seto, K. Hasimoto, H. Kominami, *Appl. Catal. A* **2013**, *450*, 28–33.
[3] a) W. Zhao, C. Liu, L. Cao, X. Yin, H. Xu, B. Zhang, *RSC Adv.* **2013**, *3*, 22944–22948; b) R. Wu, S. Wang, Y. Zhou, J. Long, F. Dong, W. Zhang, *ACS Appl. Nano Mater.* **2019**, *2*, 6818–6827.
[4] a) F. Su, S. C. Mathew, L. Möhlmann, M. Antonietti, X. Wang, S. Blechert, *Angew. Chem. Int. Ed.* **2011**, *50*, 657–660; *Angew. Chem.* **2011**, *123*, 683–

686; b) A. Kumar, P. Kumar, C. Joshi, S. Ponnada, A. K. Pathak, A. Ali, B. Sreedhar, S. L. Jain, *Green Chem.* **2016**, *18*, 2514–2521.
[5] S. Furukawa, Y. Ohno, T. Shishido, K. Teramura, T. Tanaka, *ACS Catal.* **2011**, *1*, 1150–1153.
[6] a) F. Raza, J. H. Park, H.-R. Lee, H.-I. Kim, S.-J. Jeon, J.-H. Kim, *ACS Catal.* **2016**, *6*, 2754–2759; b) H. Liang, B.-Q. Zhang, J.-M. Song, *ChemCatChem* **2019**, *11*, 6288–6294.
[7] N. Zhang, X. Li, H. Ye, S. Chen, H. Ju, D. Liu, Y. Lin, W. Ye, C. Wang, Q. Xu, J. Zhu, L. Song, J. Jiang, Y. Xiong, *J. Am. Chem. Soc.* **2016**, *138*, 8928–8935.
[8] A. Han, H. Zhang, G.-K. Chuah, S. Jaenicke, *Appl. Catal. B* **2017**, *219*, 269–275.
[9] W. Yu, D. Zhang, X. Guo, C. Song, Z. Zhao, *Catal. Sci. Technol.* **2018**, *8*, 5148–5154.
[10] a) S. Samanta, S. Khilari, D. Pradhan, R. Srivastava, *ACS Sustainable Chem. Eng.* **2017**, *5*, 2562–2577; b) K. Zhang, H. Su, H. Wang, J. Zhang, S. Zhao, W. Lei, X. Wei, X. Li, J. Chen, *Adv. Sci.* **2018**, *5*, 1800062.
[11] a) S. Naya, K. Kimura, H. Tada, *ACS Catal.* **2013**, *3*, 10–13; b) S. Sarina, H. Zhu, E. Jaatinen, Q. Xiao, H. Liu, J. Jia, C. Chen, J. Zhao, *J. Am. Chem. Soc.* **2013**, *135*, 5793–5801; c) H. Chen, C. Liu, M. Wang, C. Zhang, N. Luo, Y. Wang, H. Abroshan, G. Li, F. Wang, *ACS Catal.* **2017**, *7*, 3632–3638.
[12] a) D. Sun, L. Ye, Z. Li, *Appl. Catal. B* **2015**, *164*, 428–432; b) H. Liu, C. Xu, D. Li, H.-L. Jiang, *Angew. Chem. Int. Ed.* **2018**, *57*, 5379–5383; *Angew. Chem.* **2018**, *130*, 5477–5481.
[13] a) A. Grirrane, A. Corma, H. Garcia, *J. Catal.* **2009**, *264*, 138–144; b) L. Liu, S. Zhang, X. Fu, C.-H. Yan, *Chem. Commun.* **2011**, *47*, 10148–10150; c) X. Qiu, C. Len, R. Luque, Y. Li, *ChemSusChem* **2014**, *7*, 1684–1688; d) M. Largeron, M.-B. Fleury, *Chem. Eur. J.* **2015**, *21*, 3815–3820.
[14] a) D. Tilgner, M. Friedrich, J. Hermannsdörfer, R. Kempe, *ChemCatChem*, **2015**, *7*, 3916–3922; b) D. Tilgner, R. Kempe, *Chem. Eur. J.* **2017**, *23*, 3184–3190; c) D. Tilgner, M. Friedrich, A. Verch, N. de Jonge, R. Kempe, *ChemPhotoChem* **2018**, *2*, 349–352; d) D. Tilgner, M. Klarner, S. Hammon, M. Friedrich, A. Verch, N. de Jonge, S. Kümmel, R. Kempe, *Aust. J. Chem.* **2019**, *72*, 842–847.
[15] G. Ferey, C. Mellot-Draznieks, C. Serre, F. Millange, J. Dutour, S. Surble, I. Margiolaki, *Science* **2005**, *309*, 2040–2042.
[16] J. Hermannsdörfer, M. Friedrich, R. Kempe, *Chem. Eur. J.* **2013**, *19*, 13652–13657.
[17] a) D. Tilgner, M. Klarner, S. Hammon, M. Friedrich, A. Verch, N. de Jonge, S. Kümmel, R. Kempe, *Aust. J. Chem.* **2019**, *72*, 842–847; b) Y. Wang, Y. Zhang, Z. Jiang, G. Jiang, Z. Zhao, Q. Wu, Y. Liu, Q. Xu, A. Duan, C. Xu, *Appl. Catal. B* **2016**, *185*, 307–314; c) J. He, Z. Yan, J. Wang, J. Xie, L. Jiang, Y. Shi, F. Yuan, F. Yu, Y. Sun, *Chem. Commun.* **2013**, *49*, 6761–6763; d) D. Ding, Z. Jiang, J. Jin, J. Li, D. Ji, Y. Zhang, L. Zan, *J. Catal.* **2019**, *375*, 21–31.
[18] J. Hermannsdörfer, M. Friedrich, N. Miyajima, R. Albuquerque, S. Kümmel, R. Kempe, *Angew. Chem. Int. Ed.* **2012**, *51*, 11473–11477; *Angew. Chem.* **2012**, *124*, 11640–11644.
[19] J. Hermannsdörfer, R. Kempe, *Chem. Eur. J.* **2011**, *17*, 8071–8077.
[20] S. Proch, J. Hermannsdörfer, R. Kempe, C. Kern, A. Jess, L. Seyfarth, J. Senker, *Chem. Eur. J.* **2008**, *14*, 8204–8212.
[21] a) T. Simon, N. Bouchonville, M. J. Berr, A. Vaneski, A. Adrovic, D. Volbers, R. Wyrwich, M. Döblinger, A. S. Susha, A. L. Rogach, F. Jäckel, J. K. Stolarczyk, J. Feldmann, *Nat. Mater.* **2014**, *13*, 1013–1018; b) Y. Xu, R. Xu, *Appl. Surf. Sci.* **2015**, *351*, 779–793; c) S. Cao, C.-J- Wang, X.-J. Lv, Y. Chen, W.-F. Fu, *Appl. Catal. B* **2015**, *162*, 381–391; d) Z. Chai, T.-T. Zeng, Q. Li, L.-Q. Lu, W.-J. Xiao, D. Xu, *J. Am. Chem. Soc.* **2016**, *138*, 10128–10131; e) G. Han, Y.-H. Jin, R. A. Burgess, N. E. Dickenson, X.-M. Cao, Y. Sun, *J. Am. Chem. Soc.* **2017**, *139*, 15584–15587.
[22] A. J. Bard, M. S. Wrigthon, *J. Electrochem. Sci. Technol.* **1977**, *124*, 1706–1710.
[23] K. Ohkubo, T. Nanjo, S. Fukuzumi, *Bull. Chem. Soc. Jpn.* **2006**, *79*, 1489–1500.
[24] a) A. Henglein, *Ber. Bunsenges. Phys. Chem.* **1982**, *86*, 301–305; b) D. Meissner, C. Brenndorf, R. Memming, *Appl. Surf. Sci.* **1987**, *27*, 423–436; c) Y. H. Hsieh, C. P. Huang, *Colloids Surf.* **1991**, *53*, 275–295.
[25] J. L. DiMeglio, B. M. Bartlett, *Chem. Mater.* **2017**, *29*, 7579–7586.
[26] S. Zahner, L. Kador, K. R. Allakhverdiev, E. Yu. Salaev, M. F. Huseyinoğlu, *J. Appl. Phys.* **2014**, *115*, 043504.
[27] a) G. I. Redford, R. M. Clegg, *J. Fluoresc.* **2005**, *15*, 805–815; b) M. A. Digman, V. R. Caiolfa, M. Zamai, E. Gratton, *Biophys. J.* **2008**, *94*, L14-L16.
[28] L. Leppert, R. Kempe, S. Kümmel, *Phys. Chem. Chem. Phys.* **2015**, *17*, 26140–26148.
[29] T. Schmidt, S. Kümmel, *Computation* **2016**, *4*, 33-1–33-15.
[30] a) G. L. Gutsev, C. W. Weatherford, K. G. Belay, B. R. Ramachandran, P. Jena, *J. Chem. Phys.* **2013**, *138*, 164303; b) J. P. Chou, C. R. Hsing, C. M. Wei, C. Cheng, C. M. Chang, *J. Phys. Condens. Matter* **2013**, *25*, 125305; c) A. M. Köster, P. Calaminici, E. Orgaz, D. R. Roy, J. U. Reveles, S. N. Khanna, *J. Am. Chem. Soc.* **2011**, *133*, 12192–12196; d) B. Fresch, H.-G. Boyen, F. Remacle, *Nanoscale* **2012**, *4*, 4138–4147.
[31] TURBMOLE V7.3 **2018**, (University of Karlsruhe and Forschungszentrum Karlsruhe GmbH, Karlsruhe, Germany).
[32] a) J. P. Perdew, K. Burke, M. Ernzerhof, *Phys. Rev. Lett.* **1996**, *77*, 3865–3868; b) J. P. Perdew, K. Burke, M. Ernzerhof, *Phys. Rev. Lett.* **1997**, *78*, 1396; c) J. P. Perdew, M. Ernzerhof, *J. Chem. Phys.* **1996**, *105*, 9982; d) C. Adamo, V. Barone *J. Chem. Phys.* **1999**, *110*, 6158; e) A. D. Becke, *J. Chem. Phys.* **1993**, *98*, 5648–5652; f) P. J. Stephens, F. J. Devlin, C. F. Chabalowski, M. J. Frisch, *J. Phys. Chem.* **1994**, *98*, 11623–11627; g) J. Tao, J. P. Perdew, V. N. Staroverov, G. E. Scuseria, *Phys. Rev. Lett.* **2003**, *91*, 146401; h) V. N. Staroverov, G. E. Scuseria, J. Tao, J. P. Perdew, *J. Chem. Phys.* **2003**, *119*, 12129–12137; i) V. N. Staroverov, G. E. Scuseria, J. Tao, J. P. Perdew, *J. Chem. Phys.* **2004**, *121*, 11507–11507; j) J. Sun, A. Ruzsinszky, J. P. Perdew, *Phys. Rev. Lett.* **2015**, *115*, 036402.

Manuscript received: February 25, 2020
Revised manuscript received: June 4, 2020
Accepted manuscript online: June 5, 2020
Version of record online: ■■, ■■■

FULL PAPERS

Earth-abundant metal photocatalyst: The photocatalyst Ni/CdS@MIL-101 (MIL-101 green, CdS yellow, Ni grey) dehydrogenates benzylamine via the liberation of H_2 (amine splitting). A faster electron transfer from CdS to Ni and a stronger benzylamine binding at the Ni clusters make the earth abundant metal Ni superior in comparison to Pd and Pt.

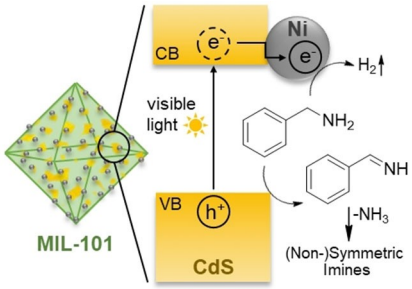

*M. Klarner, S. Hammon, S. Feulner, Prof. Dr. S. Kümmel, Prof. Dr. L. Kador, Prof. Dr. R. Kempe**